

Effect of Temperature on Tether Extraction, Surface Protrusion, and Cortical Tension of Human Neutrophils

Baoyu Liu, Craig J. Goergen, and Jin-Yu Shao

Department of Biomedical Engineering, Washington University, Saint Louis, Missouri

ABSTRACT Neutrophil rolling on endothelial cells, the initial stage of its migrational journey to a site of inflammation, is facilitated by tether extraction and surface protrusion. Both phenomena have been studied extensively at room temperature, which is considerably lower than human body temperature. It is known that temperature greatly affects cellular mechanical properties such as viscosity. Therefore, we carried out tether extraction, surface protrusion, and cortical tension experiments at 37°C with the micropipette aspiration technique. The experimental temperature was elevated using a custom-designed microscope chamber for the micropipette aspiration technique. To evaluate the constant temperature assumption in our experiments, the temperature distribution in the whole chamber was computed with finite element simulation. Our simulation results showed that temperature variation around the location where our experiments were performed was less than 0.2°C. For tether extraction at 37°C, the threshold force required to pull a tether (40 pN) was not statistically different from the value at room temperature (51 pN), whereas the effective viscosity (0.75 pN·s/μm) decreased significantly from the value at room temperature (1.5 pN·s/μm). Surface protrusion, which was modeled as a linear deformation, had a slightly smaller spring constant at 37°C (40 pN/μm) than it did at room temperature (56 pN/μm). However, the cortical tension at 37°C (5.7 ± 2.2 pN/μm) was substantially smaller than that at room temperature (23 ± 8 pN/μm). These data clearly suggest that neutrophils roll differently at body temperature than they do at room temperature by having distinct mechanical responses to shear stress of blood flow.

INTRODUCTION

Upon sensing inflammatory signals, which are usually adhesion molecules expressed on the endothelium in response to infection, neutrophils first roll on the endothelium before their firm adhesion and transmigration through the blood vessel wall. The initial rolling acts as a natural braking system to slow down neutrophils' translation in blood stream, thus assisting their ensuing firm adhesion and diapedesis. It has been well established that, during the rolling process, mechanical responses of neutrophils such as tether extraction and microvillus extension help stabilize the rolling by dramatically reducing the forces experienced by the adhesive bonds between selectins and their ligands (e.g., P-selectin and P-selectin glycoprotein ligand-1 or PSGL-1 or CD162). This increases the bond lifetime and facilitates successive bond formation (1–6). The interaction between the neutrophil and endothelium (or between the neutrophil and the substrate decorated with adhesive molecules as in many flow chamber studies) press the neutrophil against the endothelium or substrate. The contact area between the neutrophil and endothelium, which is largely determined by the neutrophil cortical tension and the interaction forces between the two cells, has been shown to be positively related to the adhesion probability between adhesive molecular pairs on neutrophils and the endothelium or substrate (7,8). Therefore, the cortical

tension is also a very important participant in regulating the complex neutrophil recruitment cascade.

Tethers are cylindrical membrane tubes with a diameter about tens of nanometers. They can be easily extracted to micrometer lengths with an appropriate point force (F) exerted on a cell membrane. It has been shown that, for a limited range of tether extraction velocity (U_t), tether extraction obeys the following relationship (9–13)

$$F = F_0 + 2\pi\mu_{\text{eff}}U_t, \quad (1)$$

where F_0 is the threshold force that needs to be overcome for a tether to be extracted, and μ_{eff} is the effective viscosity. For large U_t , a power-law relationship is more appropriate (14,15). F_0 and μ_{eff} have been reported to be ~ 45 pN and ~ 11 pN·s/μm, respectively, for passive human neutrophils (12,16,17). Tether extraction from a resting neutrophil is facilitated by the excess surface area stored in microvilli or ruffles. Microvilli are short protrusions (~ 0.3 μm) that might be supported by noncontractile actin bundles. Probed with an anti-PSGL-1-coated bead, a Hookean spring constant of 43 pN/μm was determined with the micropipette aspiration technique (MAT) under the assumption that microvilli behaved like a spring when stretched (4). Although it is disputable whether microvillus extension is only an extension in microvillus length or a combination of microvillus extension and some local cell deformation around the microvillus area, it is certain that the microvillus tip is displaced and the important implication of this phenomenon in facilitating neutrophil rolling remains. The local cell deformation may be related to cortical tension, a classical mechanical property of passive neutrophils,

Submitted January 25, 2007, and accepted for publication June 14, 2007.

Address reprint requests to Jin-Yu Shao, PhD, Dept. of Biomedical Engineering, Washington University in St. Louis, Campus Box 1097, 290E Uncas A. Whitaker Hall, One Brookings Dr., St. Louis, MO 63130-4899. Tel.: 314-935-7467; Fax: 314-935-7448; E-mail: shao@biomed.wustl.edu.

Editor: Richard E. Waugh.

© 2007 by the Biophysical Society
0006-3495/07/10/2923/11 \$2.00

doi: 10.1529/biophysj.107.105346

because cortical tension is sustained by the cytoskeletal actin filament network. The values of cortical tension of passive neutrophils documented in the literature fall in the range of 16–35 pN/ μm (18–21). Unfortunately, all these mechanical parameters were obtained at room temperature. How these mechanical properties differ at human body temperature and how they may change our understanding of neutrophil function are still unclear.

Temperature in general and body temperature in particular has a ubiquitous impact on cells. It not only affects their enzymatic activities at the molecular level (enzymes in our body function best at 37°C) but also affects their mechanical properties at the cellular and subcellular level (22–24). The fluidity of phospholipid bilayer membranes generally increases with higher temperature corresponding to a more fluid-like state. Lipid vesicle membranes tend to expand more easily with a smaller membrane expansion modulus and have lower surface shear viscosities at higher temperatures (25). Decreased extensional resistance was also observed at higher temperature in human red blood cells (24). These findings suggest that temperature has an indispensable role in characterizing membrane tether extraction. Moreover, thermodynamic studies of rabbit skeletal muscle actin polymerization showed that polymerization was enhanced at increasing temperatures (26), which suggests that temperature likely influences microvillus property and cortical tension by regulating actin filament dynamics. At higher temperature the actin filament-associated myosin in goldfish muscle cells assumes smaller sliding velocities and thus generates lower contractile tension (27). Thus, we hypothesized that cortical tension at higher temperature would be smaller than at room temperature. However, little has been done in regard to the effect of temperature on neutrophils' mechanical properties. Menasché et al. studied the influence of temperature on neutrophil trafficking in cardiopulmonary bypass and found that higher temperature (31.8°C) was advantageous for neutrophil margination over lower temperature of 26.3°C (28). Jetha et al. analyzed the ability of neutrophils to pass through micropore filters and drew the conclusion that neutrophils were more reluctant to deform upon cooling at 10°C and could recover their deformability in ~ 5 min upon rewarming to 37°C (29).

To our knowledge, there are no quantitative data available to address temperature effect on neutrophil tether extraction, surface protrusion, and cortical tension. Here, we studied these mechanical properties at both room and body temperature with the MAT aided by a heated microscope chamber. Our data showed that for tether extraction at 37°C, the threshold force had no significant deviation from that at room temperature ($\sim 22^\circ\text{C}$), whereas the effective viscosity was significantly smaller. Neutrophil surface protrusion, which was modeled as a spring-like deformation, had a smaller spring constant at 37°C than it did at room temperature. The cortical tension substantially decreased as temperature increased from room to body temperature. These results

will not only help us gain knowledge about neutrophil thermomechanics, but also help us understand neutrophil rolling *in vivo* because they clearly indicate that neutrophils roll differently at body temperature than they do at room temperature by having distinct mechanical responses to shear stress of blood flow.

METHODS AND MATERIALS

Heated microscope chamber

The heated microscope chamber (Figs. 1 and 2) consists of two integrated subunits—the experimental microscope chamber and an accompanying temperature control system. The chamber is formed by two small aluminum blocks ($31 \times 25 \times 3.2$ mm each, separated by 8 mm in between) on two sides and two glass coverslips ($15 \times 30 \times 0.32$ mm each) on the top and bottom (the chamber has two openings in the front and back). Due to its small size, the chamber can hold the cell sample inside by surface tension. The cell sample temperature is controlled by a temperature control unit, which works by a negative feedback mechanism. Several components work cooperatively to achieve a desired temperature. First, a K-gauge thermocouple (Omega, Stanford, CT) positioned in the sample solution senses the temperature at its tip. This information is then picked up by an autotuning-capable proportional-integral-derivative temperature controller (-50 – 1370°C , $\pm 0.2^\circ\text{C}$ accuracy; McMaster-Carr, Atlanta, GA). The controller will turn on (or off) the heating blankets (which are attached under the thin section of each aluminum block as shown in Fig. 1, 1 inch by 1 inch; McMaster-Carr) if the measured cell sample temperature is lower (or higher) than the set temperature. This working feedback loop can heat the chamber from a room temperature of 22 – 37°C in ~ 3 min.

Three-dimensional finite element model

To examine the temperature distribution in the heated microscope chamber, we developed a three-dimensional finite element model using ADINA

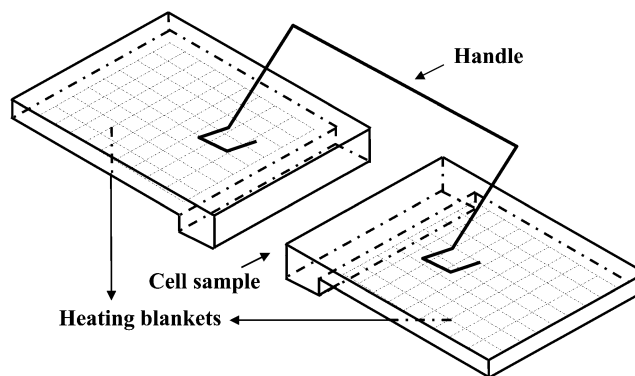


FIGURE 1 Schematic of the heated microscope chamber. Two aluminum blocks ($31 \times 25 \times 3.2$ mm each, separated by 8 mm in between), together with two glass coverslips on the top and bottom (omitted for clarity here, see Fig. 2 for their locations), forms a chamber, which holds the experimental sample. The chamber can be heated up by two electric heating blankets attached on the bottom of each aluminum block. The heating blankets, a thermocouple (which measures the cell sample temperature, not shown), and a temperature controller (which determines to heat or not according to the difference between a desired temperature and the measured temperature, not shown) work cooperatively to control the temperature in the experimental sample.

(Automatic Dynamic Incremental Nonlinear Analysis) software package (ADINA R&D, Watertown, MA). The model is described in detail in the Appendix. Briefly, the geometry of the model, which was based on a typical experiment setup, consisted of 484 points, 797 lines or curves, 475 surfaces, and 94 geometric bodies. The resulting geometric structure defined eight different units—two aluminum blocks, two glass coverslips, the experimental medium, two micropipettes, and the thermocouple (Fig. 2). The final mesh had a total node number of 14,575 and element number of 12,780. All model components were modeled as pure isotropic materials (for example, pure solid glass for the micropipette and pure solid copper for the thermocouple). The heating blankets were modeled as temperature loads applied on the aluminum blocks. For temperature boundary conditions, natural convection was used for all surfaces contacting air. Since this is a conjugate-heat-transfer problem (heat transfer in a domain that includes both fluids and solids), no temperature boundary condition was needed for the fluid-solid or solid-solid interfaces. For fluid boundary condition, no-slip was implicitly applied for all the interfaces between the medium and solid surfaces. For the two openings of the chamber, normal velocities were set to zero. Combined with the initial conditions that the temperature of the whole system was 20°C and the fluid in the chamber was at rest, this finite element problem was solved by ADINA.

Neutrophil and bead preparation

The detailed procedures for neutrophil isolation and bead preparation have been described in previous studies (12). In brief, human neutrophils from blood samples donated by healthy volunteers (by venipuncture or finger prick) were isolated with density gradient centrifugation method. The neutrophils were then suspended in 50% autologous plasma (diluted with Hanks' solution buffered with 25 mM HEPES) shortly before experiment. Latex beads (coated with goat anti-mouse antibody, ~8 μm in diameter; Sigma, St. Louis, MO) were further coated with mouse anti-human CD162 (Sigma) by incubation for ~1 h at 37°C and stored in phosphate buffered saline for later use. In surface protrusion experiments, purified general type mouse IgG (Sigma) was added to the incubation mixture to decrease the concentration of anti-CD162 on bead surfaces to achieve a low adhesion frequency between the neutrophil and bead.

Micropipette manipulation—tether extraction, surface protrusion, and cortical tension

The detailed protocols for tether extraction, surface protrusion, and cortical tension experiments have been described elsewhere (4,12,18). In brief, glass pipettes of desired inner diameter (~8 μm for bead-containing pipettes, ~4 μm for cell-holding pipettes and pipettes in cortical tension experiments) were prepared with a vertical pipette puller and a microforge. For both tether extraction and surface protrusion experiments, as shown in Fig. 3 *a*, the antibody-coated bead fit snugly inside the left pipette and acted as the force transducer of the MAT. The neutrophil, held by the smaller pipette on the right, was positioned close to the left pipette opening. A positive pressure applied inside the left pipette drove the bead into contact with the neutrophil for a short amount of time (~0.2 s). After this brief contact, a precisely

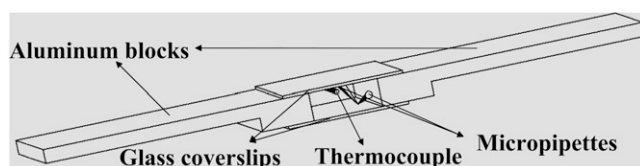


FIGURE 2 Geometric illustration of the finite element model for the heated microscope chamber. The relative positions of the micropipettes and thermocouple are shown.

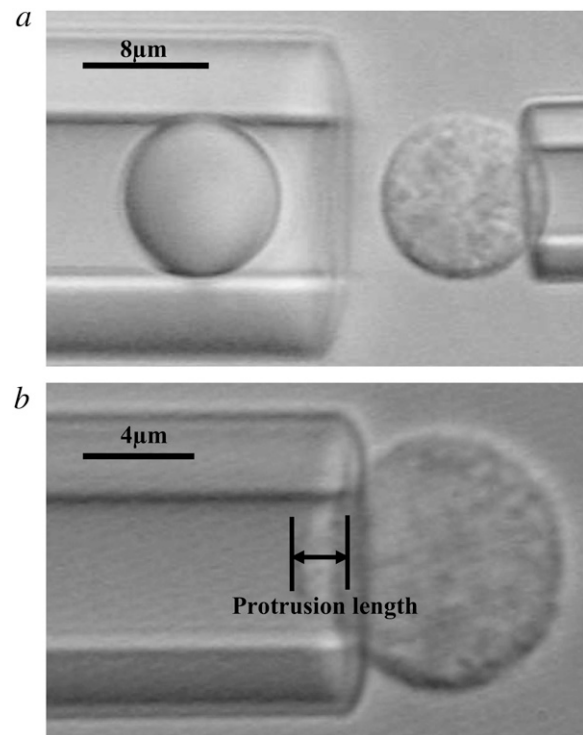


FIGURE 3 Microscopic view of tether extraction, surface protrusion, and cortical tension experiment. (*a*) The experimental setup for tether extraction from or surface protrusion of a passive neutrophil. During an experiment, the bead fit snugly inside the pipette and acted as the force transducer. The bead first approached the neutrophil on the right, made a short soft contact, and then retracted back. If adhesion occurred during contact, a tether would be extracted or neutrophil surface would deform in the course of bead retraction. (*b*) The experimental setup for measuring the cortical tension of a passive neutrophil. The suction pressure in the left pipette in a typical experiment increased from zero with an increment of 0.5 $\text{pN}/\mu\text{m}^2$. As the suction pressure increased, the projection length of the neutrophil increased accordingly. When the pressure reached a certain threshold value (the critical pressure), the projection length would be equal to the pipette radius. At this point, further pressure increase would cause the neutrophil to flow continuously into the pipette like a liquid drop. Based on the critical pressure and the corresponding projection length, the cortical tension can be calculated by the law of Laplace.

applied suction pressure replaced the positive pressure and forced the bead to return. If adhesion did not occur during contact, the bead retracted freely at a velocity, U_t , determined by the corresponding suction pressure; otherwise, the retracting velocity (U_r) would assume a smaller value (due to the pulling force applied by the neutrophil through a growing tether or a protruding cell surface. Note that $U_r = U_t$ in the case of tether extraction). The same procedures were repeated multiple times for one cell-bead pair. Experiments were recorded on a DVD and then transmitted to a PC through a monochrome frame grabber. By using an image tracking program called BeadPro8 (16), the free-motion bead velocity U_f (in the case of no adhesion) and the adhered bead velocity U_r can be obtained. Then the pulling force (F) can be calculated as follows (12):

$$F = \pi R_p^2 \Delta p \left(1 - \frac{4}{3} \frac{\varepsilon}{R_p} \right) \left(1 - \frac{U_r}{U_t} \right), \quad (2)$$

where Δp is the suction pressure applied in the left pipette of radius R_p and ε is the small gap between the force transducer and the pipette wall.

The cortical tension was measured using the method developed by Evans and Yeung (18). Briefly, the neutrophil was aspirated into a small pipette by increasing negative pressures (with an interval of $0.5 \text{ pN}/\mu\text{m}^2$; Fig. 3 b). After every suction pressure change, sufficient time ($\sim 1 \text{ min}$) was allowed for the cell to reach its new equilibrium state. Gradually, the neutrophil projection in the pipette reached the length of the pipette radius (the pressure at this point is called the critical pressure; further pressure increase will cause the neutrophil to flow into the pipette continuously). Denote the critical pressure as Δp_c , then the cortical tension (τ) can be calculated by the law of Laplace

$$\tau = \frac{\Delta p_c}{2(1/R_p - 1/R_c)}, \quad (3)$$

where R_p and R_c are the radii of the micropipette and the cell portion outside the pipette, respectively.

RESULTS

Temperature distribution in the heated chamber

All our experiments (i.e., tether extraction, surface protrusion, and cortical tension) were carried out in a small area of the microscopic view field ($\sim 300 \mu\text{m}^2$) near the micropipette tips. The micropipettes were placed at the center of the view field and close to the chamber bottom. By using the heated microscopy chamber, we wanted to control the temperature of this small area so as to ensure that our experiments were conducted at the desired temperature. However, the only position of which the exact temperature was known was at the thermocouple tip. The thermocouple was usually positioned a significant distance away from the pipette tips to avoid any disturbance from micropipette manipulation. By simulating the heated microscope chamber with finite element analysis, we obtained the temperature distribution and variation in the whole chamber. As shown in Fig. 4, the temperature at the thermocouple tip swung around 37°C (the set temperature) corresponding to the on and off

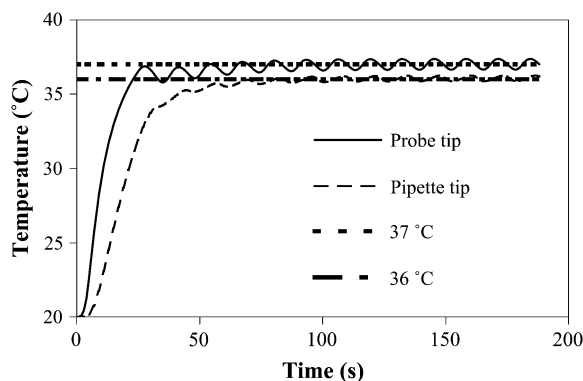


FIGURE 4 Temperature variation at the micropipette tips and the thermocouple tip. The solid black curve represents the temperature at the thermocouple tip, whereas the dashed black curve represents the temperature at the micropipette tips. The chamber was heated from room temperature to body temperature in $\sim 3 \text{ min}$; then all temperatures oscillated periodically around a certain constant value.

cycle of the heating blankets. In the meantime, the temperature around the pipette tips was varying (with a period of 13 s) around 36°C with a variance of $<0.2^\circ\text{C}$, which showed that the neutrophils in the experiments at the set temperature of 37°C were surrounded by an environment of 36°C with a small slowly changing deviation ($<0.2^\circ\text{C}$).

Another related concern in our experiments was how much the periodically varying flow field generated by thermal gradients would affect the pressure around the pipette tips. This is important because it may affect the force calculation in tether extraction and surface protrusion experiments (Eq. 2), as well as the calculation of the cortical tension (Eq. 3). Fig. 5 shows how the pressure around the micropipette tip changed over time. The maximum variance of the pressure magnitude of $\sim 0.01 \text{ pN}/\mu\text{m}^2$ was over an order of magnitude smaller than the smallest pressure drop of $0.25 \text{ pN}/\mu\text{m}^2$ used in our experiments. Therefore, we could confidently neglect the pressure variation during each thermal cycle for our force and cortical tension calculations.

Effective viscosity decreased at body temperature

With the heated microscope chamber, we performed tether extraction experiments at both room and body temperature. Fig. 6 shows a typical tracking curve of the bead displacement in our tether extraction experiments. A total of 505 and 425 tethers were extracted from passive neutrophils at room and body temperature, respectively. The collective data for the applied pulling forces and the corresponding tether extraction velocities are plotted in Fig. 7. Three different theoretical models have been proposed to describe tether extraction from cell membranes (14,15,30). To compare these models, we fitted them to the data shown in Fig. 7 and listed the obtained parameter values in Table 1. All the models fitted the data well with the two-parameter models yielding better correlation coefficients, so we chose the linear model (Eq. 1) for its ease of use. By fitting Eq. 1 to the data,

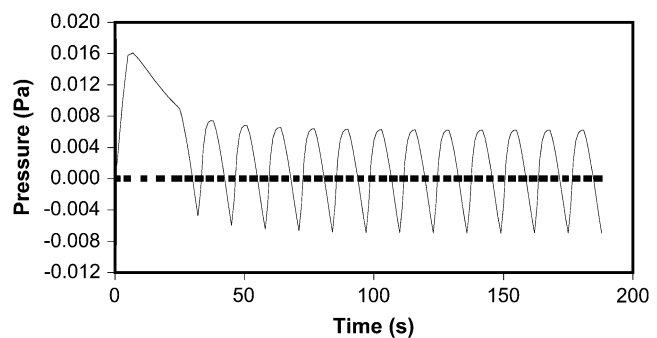


FIGURE 5 Simulated pressure variation at the micropipette tips due to the periodic heating in the microscope chamber. After the initial heating-up, the pressure oscillated periodically around zero with a maximal variance magnitude of $\sim 0.01 \text{ pN}/\mu\text{m}^2$, which is much smaller than the smallest pressure drop we used in our experiments ($0.25 \text{ pN}/\mu\text{m}^2$).

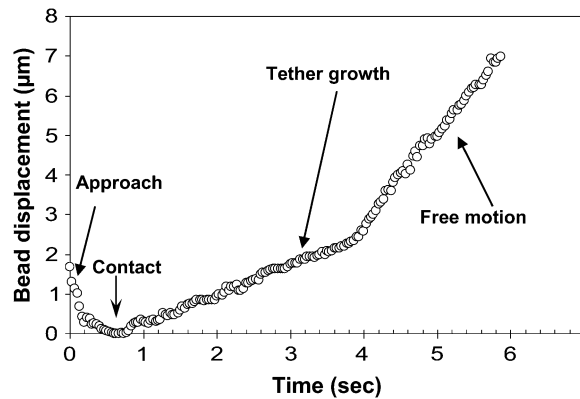


FIGURE 6 The trajectory of the force transducer (the bead) during a typical tether extraction experiment. In the case shown, the bead was driven to approach the neutrophil by a positive pressure (0–0.6 s), made a brief contact with the cell, and adhered to it (0.6–0.8 s). The bead then moved away under a suction pressure with a tether growing between the bead and neutrophil (1–4 s). Finally, after the adhesive bond broke, the bead continued to retract (4–6 s) with free motion velocity. If the bead and neutrophil did not adhere to each other, the bead would retract at its free motion velocity immediately after the contact.

we obtained the threshold forces and effective viscosities for both temperatures. The values at room temperature for the threshold force (51 pN) and effective viscosity (1.5 pN·s/μm) are comparable to those reported previously (12,17). The threshold force and effective viscosity at 37°C were 40 pN and 0.75 pN·s/μm, respectively. Statistical analysis (31) showed that the difference between the threshold forces at 22°C and 37°C was not significant ($p > 0.1$), whereas the effective viscosity at 37°C decreased significantly from the value at 22°C ($p < 0.001$). These data clearly show that, although it is equally difficult to start tethers at room and body temperature because of the similar threshold forces, they will grow much more quickly at 37°C under comparable pulling forces than they do at 22°C once initiated.

Neutrophil surface is softer at body temperature

With our temperature-control chamber, we conducted neutrophil surface protrusion experiments at both 22°C and 37°C. Since neutrophil CD162 (P-selectin glycoprotein ligand-1 or PSGL-1) molecules, which are clustered on the microvillus tips (32), interact with P-selectin during the rolling, we used anti-CD162-coated beads as the force transducer to apply pulling forces on neutrophil surfaces. The relatively long adhesion time (usually > 1 s) between the neutrophil and anti-CD162-coated beads provided us enough time to make measurements at small suction pressures (as small as 0.25 pN/μm²). By varying suction pressures used, we imposed different pulling forces on neutrophil surfaces. When the pulling force was small (< 40 pN), the neutrophil surface was only extended (Fig. 8). As the pulling force increased to > 40 pN, tethers were extracted and the percentage of tether extraction

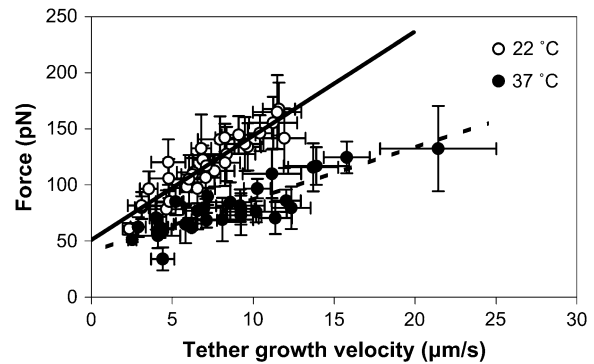


FIGURE 7 Correlation between the pulling force and tether extraction velocity for tether extraction from passive neutrophils at both 22°C and 37°C. Every point represents an average of ~ 15 tethers (the error bars represent the standard derivations), obtained with 8-μm-diameter beads and suction pressures ranging from 2 to 8 pN/μm². Effective viscosities and threshold forces at both temperatures were calculated by linear regression (the intercept corresponds to the threshold force and the slope divided by 2π corresponds to the effective viscosity). The correlation coefficients squared are 0.835 and 0.734 for these two linear regressions, respectively.

events out of all adhesion events increased as the pulling force increased. When the force was larger than ~ 70 pN, tethers were exclusively extracted without noticeable surface protrusion. A typical tracking curve for neutrophil surface protrusion is shown in Fig. 8. The retraction consists of two regions—the initial linear region (free rebound of the bead) and the later exponential region (surface protrusion). The exponential region can be described by the following empirical equation (4)

$$L = L_{\infty} - \Delta L_E e^{-t/t_c}, \quad (4)$$

where L is the total extension, L_{∞} is the equilibrium length under the pulling force, ΔL_E is the protruded length—the extensional deformation in response to the pulling force—and t_c is the characteristic time. By fitting Eq. 4 to the surface protrusion data, we obtained the protruded length (ΔL_E) for every extension event. With Eq. 2, we calculated the corresponding pulling force (at equilibrium under the pulling force where retracting velocity $U_r = 0$). A total of 75 and 108 extension events were analyzed at 22°C and 37°C, respectively. The collective data for stretching forces versus surface protrusion lengths are shown in Fig. 9. If this surface

TABLE 1 Comparison among three different tether extraction models

Model equation	α	β	Temperature	Correlation coefficient (R)
$F = \alpha U_t^\beta$	42	0.53	22°C	0.91
	31	0.46	37°C	0.84
$F = 2\pi(\alpha U_t)^{1/3}$	984	—	22°C	0.85
	275	—	37°C	0.80
$F = \alpha + 2\pi\beta U_t$	51	1.5	22°C	0.91
	40	0.75	37°C	0.86

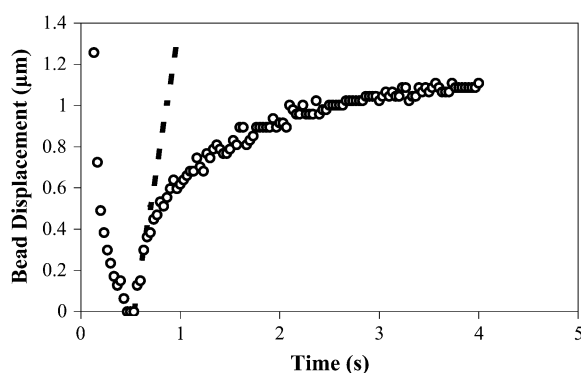


FIGURE 8 The motion of the force transducer (the bead) during a typical surface protrusion experiment. In the case shown, a positive pressure drove the bead to approach the neutrophil and make a brief contact with it during which the bead first bound to a microvillus tip through anti-CD162 and presumably pressed the microvillus down onto the cell body. Then a suction pressure forced the bead to retract back. In the meantime, the bead pulled the microvillus at its tip, causing the microvillus to quickly reach its natural length. In this first phase, because no tensile force existed in the microvillus, the bead moved back freely. The solid line represents the velocity of the same bead moving freely in the same pipette under the same suction pressure. Beyond its natural length, the microvillus and neutrophil surface were extended and gradually reached its fully extended form where the pulling force applied on the bead was balanced by the tensile force in the microvillus.

protrusion is modeled as a spring-like deformation, an apparent spring constant can be obtained by a linear fit through the origin. As shown in Fig. 9, the spring constant (the slope of the regression line) was $56 \text{ pN}/\mu\text{m}$ for 22°C and $40 \text{ pN}/\mu\text{m}$ for 37°C , which are statistically different ($p < 0.001$).

Neutrophil cortex has much more tension at room temperature

Shown in Fig. 10 are the cortical tension measurements for passive neutrophils at both room and body temperature. At 22°C , the cortical tension was $23 \pm 8 \text{ pN}/\mu\text{m}$ (mean \pm SD), which is consistent with the previously reported values (18–21). At 37°C , the cortical tension was $5.7 \pm 2.2 \text{ pN}/\mu\text{m}$. Statistic analysis showed significant difference between these two cortical tension values (two tailed Standard t -test, $p < 0.001$). During the measurement of the cortical tension, the neutrophils were aspirated into the micropipette, which caused their surface areas to increase (their volumes should be constant). However, the membrane was not expected to contribute much to the cortical tension because of the excess membrane materials stored in the microvilli and ruffles. Another possible factor that may contribute to the cortical tension is the bending of the membrane-cytoskeleton complex. Based on a model proposed by Zhelev et al. (33), this contribution should be negligible because the pipette radii used in our experiments ($\sim 2 \mu\text{m}$) were large enough. Therefore, the major determinant of the cortical tension is very likely the underlying actin cortex, which

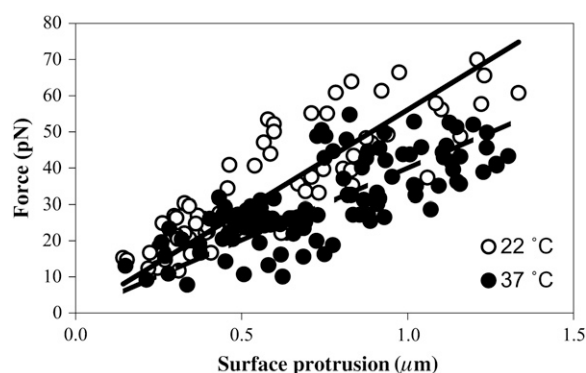


FIGURE 9 Correlation between the pulling force and surface protrusion at 22°C and 37°C . Every point (an open circle or a solid circle) represents one surface protrusion of a cell for which we calculated the force according to Eq. 2 and obtained the extended length from fitting Eq. 4 to the extension data. Linear regression through the origin gave spring constants at both temperatures. Slightly different spring constants were obtained ($46 \text{ pN}/\mu\text{m}$ and $30 \text{ pN}/\mu\text{m}$ at 22°C and 37°C , respectively) if linear regression was not forced to go through the origin.

probably became more flexible in response to temperature increase in our experiments at 37°C (34).

DISCUSSION

Temperature plays a central role in every aspect of cellular life. Human neutrophils, one of the key components of our immune defense system, presumably function best at our body temperature. However, most mechanical studies of neutrophils have been performed at room temperature. To address this issue, we studied three mechanical properties of neutrophils that are essential for understanding neutrophil migration to inflammatory sites—tether extraction, surface protrusion, and cortical tension—using the MAT and a heated microscope chamber. Significant difference was found in all these properties at body temperature compared with room temperature. Our results showed that, at body temperature, tethers were more readily to be extracted from neutrophils, neutrophil surfaces were easier to deform, and the cortical tension was much smaller. These findings have important implications for modeling neutrophil behavior in vivo and will also help us understand how neutrophils function in vivo, especially in regard to rolling on the endothelium.

The heated microscope chamber was custom-made for the sole purpose of temperature control, so any other side effect on neutrophils is undesirable. However, the electricity-powered heating system may create some potential gradients between the two aluminum blocks. Considering the short separation distance between the two blocks ($\sim 8 \text{ mm}$), the resulting electrical field in the chamber may have considerable effect on neutrophils. To eliminate this possible effect, we shorted the two aluminum blocks and grounded them during our experiments. Furthermore, we examined the

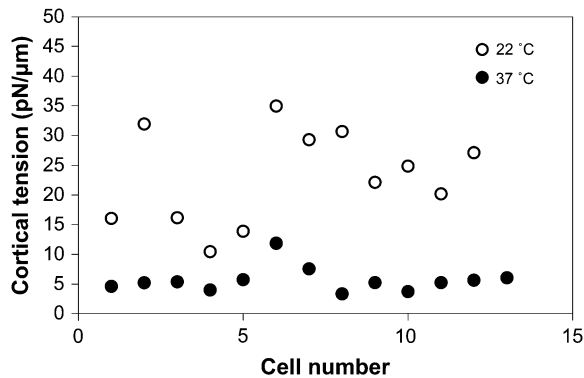


FIGURE 10 Cortical tension of passive neutrophils at 22°C and 37°C. Every point shown here corresponds to one measurement from one neutrophil. The average value at 22°C was 23 pN/μm with a standard deviation of 8 pN/μm, whereas the average value at 37°C was 5.7 pN/μm with a standard deviation of 2.2 pN/μm.

effects of electric fields on neutrophils in two separate experiments. First, using optical tweezers, we did force relaxation experiments for several tethers extracted from passive neutrophils at 37°C during which we turned on and off the heating blankets (with each state kept for ~ 2 s). Sudden transmembrane potential change should lead to sudden tether force change (35), but no discernible force jumps were observed when the heating blankets were turned on or off. Secondly, we measured the cortical tension of neutrophils when heating was either on or off at room temperature and we found no significant difference between the values under both conditions (data not shown). Therefore, we concluded that our measurements at body temperature were free of electrical effects on neutrophils.

Tether extraction from passive neutrophils has been studied extensively at room temperature using the micropipette aspiration technique (12,16,17). Mechanically characterized by the threshold force and effective viscosity, tether extraction has been shown to be independent of adhesion molecules used to apply pulling forces, which is indicative of an intrinsic membrane protrusion process. However, there was a lack of knowledge about how tether extraction is regulated by temperature. Here, for the first time, we reported the threshold force (40 pN) and effective viscosity (0.75 pN·s/μm) for tether extraction from passive neutrophils at 37°C. According to Waugh et al. (24), the area expansion modulus of erythrocyte membranes (K) decreased $\sim 20\%$ from 22°C to 37°C. Coincidentally, F_0 also decreased $\sim 20\%$ from 22°C to 37°C. Higher temperature is accompanied by more vigorous thermal agitation of lipid molecules, resulting in weakened interactions among lipid molecules, thus decreasing K . However, the higher temperature of 37°C did not result in statistically different threshold force whereas it did result in significant lower effective viscosity. Caution should be taken in claiming that these two threshold forces are not different because we did not measure them directly.

Because of the transition from surface protrusion to tether extraction, we could not obtain data points with small tether extraction velocities to avoid any biased data samples at small suction pressures. This is why large uncertainty might be involved with the prediction of the intercepts. Until the threshold force is measured directly, this conclusion should be applied with caution. For cells with excess membrane stored in microvilli such as neutrophils, the threshold force (F_0) is mainly determined by the membrane-cytoskeleton adhesion energy, membrane tension, and membrane bending (30). For neutrophils, the estimated membrane-cytoskeleton adhesion energy of ~ 130 pN/μm (36) is about four or five times the cortical tension of ~ 25 pN/μm, which includes both the cortex and membrane contribution with the cortex playing a dominant role. Because lipid bilayers with cholesterol have a bending modulus (B) of ~ 0.2 pN·μm (37), the contribution from membrane bending to the threshold force is ~ 20 pN for a tether radius of 0.03 μm.

The effective viscosity (μ_{eff}) at 37°C almost decreased by half from the value at 22°C. Three major contributors to the effective viscosity are the membrane flow, the interlayer slip, and the membrane slip over the cytoskeleton (30). Our results indicate that the temperature increase led to smaller viscosities of cytoplasm and membrane lipids, which may be attributed to two sources. First, the membrane-spanning integral proteins that are linked to the cytoskeleton provide much resistance for the membrane flow and the membrane slip over the cytoskeleton. As a tether grows, cell membrane flows continuously into it, leaving the cytoskeleton behind. The membrane slip over the cytoskeleton might rupture the binding between the proteins and cytoskeleton. On the other hand, the membrane might just slide around proteins without disrupting their connections with the cytoskeleton. Higher temperature of 37°C presumably decreased the slip resistance by elevating lipid molecules' mobility and by decreasing the anchoring strength of integral proteins to the cytoskeleton with more thermal agitation. Secondly, higher temperature tends to weaken the interactions between lipid molecules and their interactions with the cytoskeleton, resulting in decreased friction and increased fluidity from 22 to 37°C. For neutrophil flow into glass tubes, their apparent viscosity decreased from 2000 poise at 23°C to 1000 poise at 37°C (18). Although there is no direct measurement of the neutrophil membrane viscosity at room and body temperature, there is a study on the temperature dependence of the viscosity of a synthetic biomembrane with cholesterol:DMPC equal to 0.3. This work showed a twofold increase in the diffusion coefficient upon a temperature increase from 20°C to 35°C (38), indicating that neutrophil membrane viscosity at 22°C was roughly halved when temperature increased to 37°C.

In our neutrophil surface protrusion experiments, we applied pulling forces on microvilli tips via CD162. The microvilli tip displacement was inferred by the anti-CD162-coated bead movement. After the free rebound, the force would displace the microvilli tip. This displacement was

modeled as a spring-like deformation, which may attribute to both microvillus extension and cytoskeletal deformation. In a previous study (4), it was assumed that the junction between the microvillus and the neutrophil body was fixed, thus the recorded microvillus tip displacement reflected only microvillus extension. However, since microvilli may be supported by actin filaments whose extensional stiffness is much larger than the calculated microvillus spring constant and these actin filaments are connected to the cell body, the measured microvillus extension might also involve additional local cell body deformation around the junction. This is a complicated scenario where a clear understanding is not yet known. We can only postulate that the membrane is likely extended first, with the actin filaments becoming aligned with the pulling direction. Then the fully extended actin filaments would pull on the cytoskeleton and cause a certain amount of cell body deformation. This is why we have termed this displacement as surface protrusion rather than microvillus extension. Whether it is microvillus extension or local cell body deformation or both, the significance of the microvillus tip displacement in stabilizing neutrophil rolling remains the same. Thus, in retrospect, the simplification of using one spring constant to characterize this neutrophil response is a simple and effective way of incorporating mechanical response in understanding the rolling process. Our data showed that the measured spring constant was smaller at 37°C (40 pN/ μ m) than at 22°C (56 pN/ μ m), indicating microvillus tips are more easily displaced under pulling forces *in vivo* than at room temperature. The difference between the two spring constants at 22°C and 37°C may be due to different membrane fluidity, different organization or polymerization rate of supporting actin filaments, or even different mechanical properties of the whole cell at the two studied temperatures. Our value of 56 pN/ μ m at 22°C is slightly larger than the value determined previously with the same technique (4), probably because more data points were collected in this study, thus resulting in a more accurate measurement, and the linear regression performed by Shao et al. (4) was not forced to go through the origin.

We obtained significantly smaller cortical tension at 37°C than at 22°C. The cortical tension is mainly maintained by the cytoskeleton and is likely generated by myosin molecules cross-linking neighboring actin filaments as in *dictyostelium discoideum* (39). Our data suggest that the actin filaments in neutrophils behave like those in rabbit skeletal muscles with higher turnover rate at higher temperature (26) and the myosin in neutrophils is regulated by temperature in a similar way as in goldfish muscle cells with smaller sliding velocities (and thus smaller tension) at higher temperature (27). It has also been shown that some regions of the catalytic domain of the myosin from rabbit muscle can have very different conformations and functions at different temperatures (40). The approximately fourfold smaller cortical tension at 37°C (5.7 pN/ μ m) than at 22°C (23 pN/ μ m) was striking for a temperature difference of 15°C. This finding may have important implications in understanding neutro-

phil behaviors *in vivo*, since cortical tension influences a variety of neutrophil-related processes. For example, cortical tension is an important parameter in modeling neutrophil phagocytosis (41). The smaller cortical tension at body temperature would make it easier for neutrophils to phagocyte invading microorganisms. Also, with smaller cortical tension, the floppy neutrophils could move more easily through individual capillary vessels. In fact, Jehta et al. studied neutrophils' passage through microvessels (with a diameter of either 5 or 8 μ m) at both 10°C and 37°C and found that neutrophils could block the microvessels at the lower temperature and regain the ability of passage upon warming to the higher temperature (29). Another finding by Jehta et al. was that the F-actin contents at two temperatures were at the same level. Thus the higher resistance at lower temperature was likely because of the higher rigidity of the F-actin scaffolding. A plausible explanation of the rigidity variation at different temperatures is the different polymerization rate of the actin filaments as seen in rabbit skeletal muscles. This is the most likely reason for the cortical tension difference at 22°C and 37°C.

Both the surface protrusion and cortical tension measurements involve cell surface area increase, i.e., surface extension. This may suggest a possible connection between the cortical tension and the spring constant of surface protrusion. However, the cortical tension only depends weakly on surface extension (33,42) and the cell deformation during the surface protrusion generated by a point force is invisible under a microscope, implying very small surface extension, if any. The spring constant of surface protrusion is directly related to the bending rigidity of the cortex, which is a material constant; while the cortical tension is probably the response of the cortex to the pressure difference inside and outside the cell. Consequently, our experimental data did not allow us to establish any connection between the cortical tension and the spring constant of surface protrusion through surface extension although they might be correlated in some other fashion.

Tether extraction and surface protrusion are two major mechanical means employed by neutrophils to stabilize the initial rolling process in their recruitment cascade. It is well known that both tether extraction and surface protrusion can act to decrease the hydrodynamic shear force exerted on the adhesive bonds by lengthening the momentum arm (the lateral distance between the attachment point and the center of cell-surface contact) (4,6). Our data indicate that under the same flow condition, the momentum arm, which is determined by surface protrusion and tether flow, can be increased more rapidly at body temperature. Spillmann et al. have demonstrated that the rate of bond formation between β_2 -integrin on neutrophils and immobilized ICAM-1 increases linearly with contact area between the neutrophil and the ICAM-1-coated substrate (8). Therefore, smaller cortical tension *in vivo* could facilitate neutrophils' attachment on the endothelium in their process of transmigration by

providing a relatively larger contact area, especially during the later stage of rolling and firm adhesion. These findings should provide more relevant parameters for modeling neutrophil processes and help us understand neutrophil functions at their natural environment of 37°C.

APPENDIX: THREE-DIMENSIONAL FINITE ELEMENT ANALYSIS OF THE HEATED MICROSCOPE CHAMBER

THEORETICAL FORMULATION

Geometry

The model was developed with ADINA, a finite element analysis software package for structures, heat transfer, and fluid dynamics (ADINA R&D). As shown in Figs. 1 and 2, the model consisted of eight parts—two aluminum blocks (left and right, $31 \times 25 \times 3.2$ mm each), two glass coverslips (top and bottom, $15 \times 25 \times 0.32$ mm each), one experimental medium sample, two micropipettes, and a thermocouple (a 12.5-mm long copper cylinder with a diameter of 0.5 mm). The aluminum blocks and the glass coverslips formed the chamber ($8 \times 25 \times 3.2$ mm). This chamber was filled with the experimental medium, micropipettes, and temperature probe. Each glass pipette was modeled as a truncated cone (with diameters of 10 μ m and 0.8 mm at two ends and length of 12.5 mm). The two micropipettes were immersed in the experimental medium with their two larger ends located at the front and back surface of the medium, respectively. The larger ends entered the chamber midway between the two coverslips, where the tips were positioned close to the bottom coverslip. To avoid disturbing micropipette manipulation, the thermocouple was positioned a small distance away from the experimental location. The total dimensions of the model were 70 mm (length) \times 25 mm (width) \times 3.84 mm (height).

Governing equations

This is a heat transfer problem in a domain that includes both fluid and solid materials, the so-called conjugate heat transfer problem. The heat transfer in the fluid (i.e., the experimental medium) occurs by convection and conduction, whereas the heat transfer in the solids occurs by conduction only. For the fluid subdomain, the Boussinesq approximation was used. This approximation states that 1), fluid density ρ varies linearly with temperature; and 2), the variable density ρ can be replaced everywhere by a constant reference value ρ_0 except in the buoyancy force term $(\rho - \rho_0)\vec{g}$ where \vec{g} is the gravitational acceleration vector. With this approximation, the continuity, momentum, and energy equations can be written as follows,

$$\nabla \cdot \vec{v} = 0, \quad (\text{A-1})$$

$$\frac{\partial \vec{v}}{\partial t} + \vec{v} \cdot \nabla \vec{v} = -\frac{\nabla \phi}{\rho_0} - \vec{g}\beta(T - T_0) + \frac{\mu}{\rho_0} \nabla^2 \vec{v}, \quad (\text{A-2})$$

$$\frac{\partial T}{\partial t} + \vec{v} \cdot \nabla T = \frac{k}{\rho_0 C_p} \nabla^2 T, \quad (\text{A-3})$$

where \vec{v} , ϕ , ρ_0 , β , μ , T , T_0 , k , and C_p are velocity vector, dynamic pressure, reference density, thermal expansion coefficient, viscosity, temperature, reference temperature, thermal conductivity, and specific heat, respectively. In Eq. A-3, two terms of mechanical effects were ignored, both of which would appear as additional energy sources. One was the viscous dissipation—the heat generated due to internal fluid friction. This was negligible because velocity scale in this model would be small (the characteristic velocity was estimated to be about 0.01 m/s) and the medium in the chamber was not highly viscous (43). The other neglected term is

related to the work done in compressing the fluid, which was omitted based on the Boussinesq approximation.

The governing equations for the heat transfer in the solids are reduced to Eq. A-3 only. However, for convenience, the same set of equations (A-1–A-3) were used for the solids. Special consideration was given such that their velocity degrees of freedom were automatically deleted including solid-fluid interfaces and their pressure degrees of freedom were also removed except on solid-fluid interfaces. This way, the whole domain can be solved simultaneously. In the fluid subdomain, ρ_0 , β , μ , T_0 , k , and C_p were equal to 993 kg·m⁻³, 0.00036 K⁻¹, 0.00098 kg·m⁻¹·s⁻¹, 310 K, 0.625 W·K⁻¹·m⁻¹, and 4182 J·kg⁻¹·K⁻¹, respectively. For glass coverslips and micropipettes, $\rho = 2240$ kg·m⁻³, $k = 1.09$ W·K⁻¹·m⁻¹, $C_p = 840$ J·kg⁻¹·K⁻¹. For aluminum blocks, $\rho = 2700$ kg·m⁻³, $k = 237$ W·K⁻¹·m⁻¹, $C_p = 900$ J·kg⁻¹·K⁻¹. For the copper thermocouple, $\rho = 8920$ kg·m⁻³, $k = 401$ W·K⁻¹·m⁻¹, and $C_p = 380$ J·kg⁻¹·K⁻¹.

Heat load

Due to the feedback control of the heating system, dynamic analysis must be used to solve this heat transfer problem. The rise and fall of the temperature in the whole domain is determined by how the heat is administrated though the two heating blankets attached firmly and uniformly under the two aluminum blocks. The heating from the blankets was modeled as prescribed temperature variations of the attached blankets on the aluminum blocks. Shown in Fig. 11 are the measured temperature variations of the heating blankets or heat loads in our model. We assumed the same temperature variations on the heating blankets and the aluminum block surfaces covered by the blankets—the outer thinner sections as shown in Fig. 12.

Initial conditions

At the start of the simulation, temperature in the whole domain was set to 20 °C and the medium in the chamber was at rest (no flow).

Boundary conditions

For a conjugate heat transfer problems in ADINA, since the fluid and solids are considered as a whole to solve, the interfaces between the fluid and solids are not treated as boundaries. Therefore, velocity boundary conditions are only needed on the front and back surfaces of the medium, where normal component of the velocity was set to zero.

For temperature boundary conditions, natural convection was used for all exterior surfaces contacting air. In this condition, the heat fluxes q_n on the model surfaces are proportional to the temperature difference between the model surfaces and the environment,

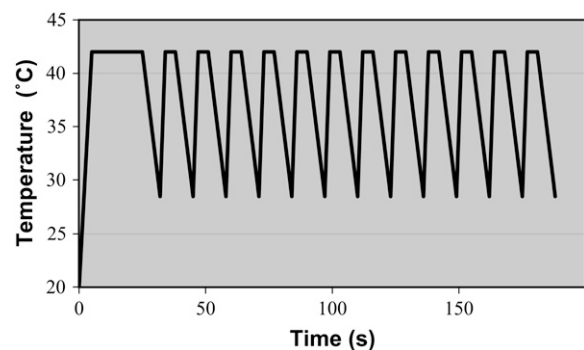


FIGURE 11 The heat load prescribed on the bottom surfaces of the aluminum blocks, which were measured with an infrared thermometer.

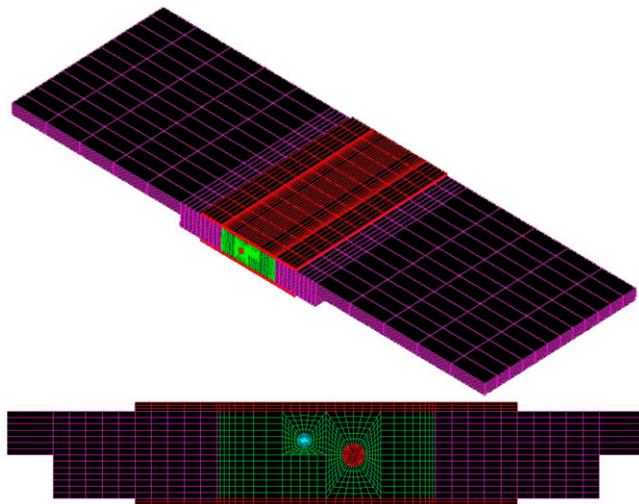


FIGURE 12 The mesh generated in the simulation. The upper panel shows the three-dimensional view of the mesh and the lower one shows the zoom-in front view (only parts of the aluminum blocks are shown in the lower panel). Different line colors indicate different materials with green for the experimental medium, blue for the thermocouple, red for the glass coverslips and micropipettes, and purple for the aluminum blocks.

$$q_n = h \times (T - T_e) = h \times \Delta T, \quad (\text{A-4})$$

where h is the heat convection coefficient and T_e is the ambient temperature. The heat convection coefficient h has different empirical expressions for vertical and horizontal surfaces. For vertical surfaces,

$$h = 1.42 \times \left(\frac{\Delta T}{L_v} \right)^{1/4}, \quad (\text{A-5})$$

where L_v is the characteristic length of the vertical surface (44). For horizontal surfaces,

$$h = 1.32 \times \left(\frac{\Delta T}{L_h} \right)^{1/4}, \quad (\text{A-6})$$

where L_h is the characteristic length of the horizontal surface (44). For the fluid subdomain, prescribed boundary conditions were all velocity and temperature conditions. Thus, in order for the pressure solution to be completed, zero pressure was imposed at the bottom-left point of the chamber medium.

Numerical computation

Combined with the heat load, initial condition, and boundary conditions, Eqs. A-1–A-3 can be solved with ADINA. In ADINA, geometry definition, mesh generation, problem definition, boundary condition application, solution, and postprocessing can be carried out in a single integrated platform called ADINA-AUI. The model geometry consisted of 484 points, 797 lines (or curves), 475 surfaces, and 94 geometric bodies. For meshing, the major element type was eight-node brick except the pipettes and thermocouple for which six-node prism was used. Mesh generation was done in such a way that desired mesh densities were achieved in selected regions. For example, finer meshes were used in the fluid subdomain for the regions close to the solid walls since dramatic velocity variations are expected there; for the aluminum blocks, finer meshes were generated for the sections close to the chamber since temperature variations are expected to be large there. The final mesh (Fig. 12) had a total node number of 14,575 and element number of 12,780.

Based on the generated meshes, ADINA-F (a module for analyzing fluid-flow problems) then generated the finite element equations through discretization of the governing equations. The resulting algebraic equations formed a coupled system of all solution variables (\vec{v} , ρ , T) for all nodal points. Due to the high nonlinearity of the problem, it was solved by an incremental/iterative scheme. For every time instant t (the chosen time step Δt was 1 s), the procedure for obtaining the solution at $t + \Delta t$ started from the solution at the last time instant (at time t) as the initial guess. A solution increment was obtained from the linearized system and the solution was updated by summing the increment and the previous value. Then the following convergence criterion was checked,

$$\max_f \left\{ \frac{\|\Delta X_f\|}{\|X_f\|} \right\} < \varepsilon, \quad (\text{A-7})$$

where $f = \vec{v}, \rho$, or T and ΔX_f is the increment vector and X_f is the updated solution vector for variable f , ε is a preset tolerance (adjusted by ADINA-F), and the norm $\|\cdot\|$ is the Euclidean norm. If the criterion was satisfied, the solution at $t + \Delta t$ was obtained; otherwise, taking the updated solution as the next guess, the same procedure was repeated (iteration). In solving the linearized equations, the sparse solver in ADINA-F was used. The sparse solver is a direct solver based on the Gauss elimination method and greatly improves solution efficiency by preserving the sparsity of the matrix, thus reducing the storage and computation time. To improve the matrix conditioning, nondimensionalization was used by choosing proper scales for density, length, velocity, temperature, and specific heat according to the ADINA theory and modeling guide.

To complete the simulation corresponding to the heat loads of 188 s, it took roughly 12 h of CPU time (Intel Pentium, 3.0 GHz, 2 GB memory). After obtaining the solution, the simulation results such as velocity, pressure, and temperature were retrieved and analyzed using the postprocessing module, ADINA-PLOT.

This work was supported by the National Heart, Lung and Blood Institute (grant No. R01 HL069947) and the National Center for Research Resources (grant No. R21/R33 RR017014).

REFERENCES

- Girdhar, G., and J.-Y. Shao. 2004. Membrane tether extraction from human umbilical vein endothelial cells and its implication in leukocyte rolling. *Biophys. J.* 87:3561–3568.
- Park, E. Y., M. J. Smith, E. S. Stropp, K. R. Snapp, J. A. DiVietro, W. F. Walker, D. W. Schmidtke, S. L. Diamond, and M. B. Lawrence. 2002. Comparison of PSGL-1 microbead and neutrophil rolling: microvillus elongation stabilizes P-selectin bond clusters. *Biophys. J.* 82:1835–1847.
- Ramachandran, V., M. Williams, T. Yago, D. W. Schmidtke, and R. P. McEver. 2004. Dynamic alterations of membrane tethers stabilize leukocyte rolling on P-selectin. *Proc. Natl. Acad. Sci. USA.* 101:13519–13524.
- Shao, J.-Y., H. P. Ting-Beall, and R. M. Hochmuth. 1998. Static and dynamic lengths of neutrophil microvilli. *Proc. Natl. Acad. Sci. USA.* 95:6797–6802.
- Schmidtke, D. W., and S. L. Diamond. 2000. Direct observation of membrane tethers formed during neutrophil attachment to platelets or P-selectin under physiological flow. *J. Cell Biol.* 149:719–729.
- Yu, Y., and J.-Y. Shao. 2007. Simultaneous tether extraction contributes to neutrophil rolling stabilization: a model study. *Biophys. J.* 92:418–429.
- Lomakina, E. B., and R. E. Waugh. 2004. Micromechanical tests of adhesion dynamics between neutrophils and immobilized ICAM-1. *Biophys. J.* 86:1223–1233.
- Spillmann, C. M., E. Lomakina, and R. E. Waugh. 2004. Neutrophil adhesive contact dependence on impingement force. *Biophys. J.* 87:4237–4245.

9. Dai, J., and M. P. Sheetz. 1995. Regulation of endocytosis, exocytosis, and shape by membrane tension. *Cold Spring Harb. Symp. Quant. Biol.* 60:567–571.
10. Evans, E., and A. Yeung. 1994. Hidden dynamics in rapid changes of bilayer shape. *Chem. Phys. Lipids.* 73:39–56.
11. Li, Z., B. Anvari, M. Takashima, P. Brecht, J. H. Torres, and W. E. Brownell. 2002. Membrane tether formation from outer hair cells with optical tweezers. *Biophys. J.* 82:1386–1395.
12. Shao, J.-Y., and R. M. Hochmuth. 1996. Micropipette suction for measuring piconewton forces of adhesion and tether formation from neutrophil membranes. *Biophys. J.* 71:2892–2901.
13. Waugh, R. E., and R. G. Bauserman. 1995. Physical measurements of bilayer-skeletal separation forces. *Ann. Biomed. Eng.* 23:308–321.
14. Brochard-Wyart, F., N. Borghi, D. Cuvelier, and P. Nassoy. 2006. Hydrodynamic narrowing of tubes extruded from cells. *Proc. Natl. Acad. Sci. USA.* 103:7660–7663.
15. Heinrich, V., A. Leung, and E. Evans. 2005. Nano- to microscale dynamics of P-selectin detachment from leukocyte interfaces. II. Tether flow terminated by P-selectin dissociation from PSGL-1. *Biophys. J.* 88:2299–2308.
16. Shao, J.-Y., and J. Xu. 2002. A modified micropipette aspiration technique and its application to tether formation from human neutrophils. *J. Biomech. Eng.* 124:388–396.
17. Xu, G., and J.-Y. Shao. 2005. Double tether extraction from human neutrophils and its comparison with CD4+ T-lymphocytes. *Biophys. J.* 88:661–669.
18. Evans, E., and A. Yeung. 1989. Apparent viscosity and cortical tension of blood granulocytes determined by micropipette aspiration. *Biophys. J.* 56:151–160.
19. Lomakina, E. B., C. M. Spillmann, M. R. King, and R. E. Waugh. 2004. Rheological analysis and measurement of neutrophil indentation. *Biophys. J.* 87:4246–4258.
20. Needham, D., and R. M. Hochmuth. 1992. A sensitive measure of surface stress in the resting neutrophil. *Biophys. J.* 61:1664–1670.
21. Tsai, M. A., R. S. Frank, and R. E. Waugh. 1994. Passive mechanical behavior of human neutrophils: effect of cytochalasin B. *Biophys. J.* 66:2166–2172.
22. Hochmuth, R. M., K. L. Buxbaum, and E. A. Evans. 1980. Temperature dependence of the viscoelastic recovery of red cell membrane. *Biophys. J.* 29:177–182.
23. Nash, G. B. 1985. Alteration of red cell membrane viscoelasticity by heat treatment: effect on cell deformability and suspension viscosity. *Biorheology.* 22:73–84.
24. Waugh, R. E., and E. Evans. 1979. Thermoelasticity of red blood cell membrane. *Biophys. J.* 26:115–132.
25. Evans, E., and D. Needham. 1987. Physical properties of surfactant bilayer membranes: thermal transitions, elasticity, rigidity, cohesion and colloidal interactions. *J. Phys. Chem.* 91:4219–4228.
26. Asakura, S., M. Taniguchi, and F. Oosawa. 1963. Mechano-chemical behaviour of F-actin. *J. Mol. Biol.* 7:55–69.
27. Watabe, S. 2002. Temperature plasticity of contractile proteins in fish muscle. *J. Exp. Biol.* 205:2231–2236.
28. Menasché, P., J. Peynet, N. Haeflner-Cavaillon, M. P. Carreno, T. de Chaumaray, V. Dillisse, B. Faris, A. Piwnica, G. Bloch, and A. Tedgui. 1995. Influence of temperature on neutrophil trafficking during clinical cardiopulmonary bypass. *Circulation.* 92:334–340.
29. Jetha, K. A., S. Egginton, and G. B. Nash. 2003. Increased resistance of neutrophils to deformation upon cooling and rate of recovery on rewarming. *Biorheology.* 40:567–576.
30. Hochmuth, R. M., J.-Y. Shao, J. Dai, and M. P. Sheetz. 1996. Deformation and flow of membrane into tethers extracted from neuronal growth cones. *Biophys. J.* 70:358–369.
31. Zar, J. H. 1999. Biostatistical Analysis. Prentice Hall, Upper Saddle River, NJ.
32. Moore, K. L., K. D. Patel, R. E. Bruehl, F. Li, D. A. Johnson, H. S. Lichenstein, R. D. Cummings, D. F. Bainton, and R. P. McEver. 1995. P-selectin glycoprotein ligand-1 mediates rolling of human neutrophils on P-selectin. *J. Cell Biol.* 128:661–671.
33. Zhelev, D. V., D. Needham, and R. M. Hochmuth. 1994. Role of the membrane cortex in neutrophil deformation in small pipets. *Biophys. J.* 67:696–705.
34. Tsai, M. A., R. E. Waugh, and P. C. Keng. 1998. Passive mechanical behavior of human neutrophils: effects of colchicine and paclitaxel. *Biophys. J.* 74:3282–3291.
35. Qian, F., S. Ermilov, and D. Murdock. 2006. Combining optical tweezers and patch clamp for studies of cell membrane electro-mechanics. *Rev. Sci. Instrum.* 75:2937–2942.
36. Hochmuth, R. M., and W. D. Marcus. 2002. Membrane tethers formed from blood cells with available area and determination of their adhesion energy. *Biophys. J.* 82:2964–2969.
37. Waugh, R. E., and R. M. Hochmuth. 1995. Mechanics and deformability of hematocytes. In *The Biomedical Engineering Handbook*. J. D. Bronzino, editor. CRC Press, Boca Raton, FL. 474–486.
38. Bossev, D. P., and N. S. Rosov. 2003. Bio-membrane flexibility studied in the presence of cholesterol and salt. *NIST Center for Neutron Research Annual Report.* 18–19.
39. Dai, J., H. P. Ting-Beall, R. M. Hochmuth, M. P. Sheetz, and M. A. Titus. 1999. Myosin I contributes to the generation of resting cortical tension. *Biophys. J.* 77:1168–1176.
40. Nitao, L. K., and E. Reisler. 2000. Actin and temperature effects on the cross-linking of the SH1-SH2 helix in myosin subfragment 1. *Biophys. J.* 78:3072–3080.
41. Herant, M., V. Heinrich, and M. Dembo. 2005. Mechanics of neutrophil phagocytosis: behavior of the cortical tension. *J. Cell Sci.* 118:1789–1797.
42. Drury, J. L., and M. Dembo. 2001. Aspiration of human neutrophils: effects of shear thinning and cortical dissipation. *Biophys. J.* 81:3166–3177.
43. Deen, W. M. 1998. Analysis of Transport Phenomena. Oxford University Press, New York.
44. Holman, J. P. 1981. Heat Transfer. McGraw-Hill Book Company, Mallik, AK.